Elastic Scattering of O^{16} by Ti^{48}, Ca^{40}, Al^{27}, C^{12}, Li^{7}, and Li^{6}†

J. Orloff and W. W. Daehnick
Nuclear Physics Laboratory, University of Pittsburgh, Pittsburgh, Pennsylvania 15213
(Received 28 September 1970)

A number of isotopically enriched light targets were bombarded with O^{16} ions of 36- to 48-MeV energy (lab), and ten elastic angular distributions were measured. All cross sections show strongly destructive interference of nuclear and Coulomb scattering at angles above 30 to 60° c.m., and fall orders of magnitude below the Coulomb cross section. The data were fitted reasonably well with conventional optical-model calculations, and $\langle\chi^2\rangle$ values between 0.5 and 5.2 could be obtained for all targets. Typically, four-parameter fits were adequate. For the heavier targets the parameter sets are not unique, but were found to have continuous well-depth–geometry ambiguities, which were investigated in some detail. A procedure to produce *in situ* clean targets of highly reactive elements is described.

I. INTRODUCTION

Increasingly, heavy projectiles – in particular, $Li^{6,7}$ and O^{16} ions – are used to induce nuclear reactions, the analysis of which usually requires the knowledge of the scattered-projectile waves. Compared with other projectiles, little information exists on elastic O^{16} scattering, and the present study was undertaken as a step towards accumulating more comprehensive empirical information on scattering by lighter targets where significant deviations from simple Coulomb scattering are expected, even at relatively low energies.

It has been argued that the optical model in its conventional form is not well suited to explain the observed angular distributions for heavy ions.[1,2] Nevertheless, with the exception of C^{12}, good fits can be obtained for the targets investigated, and it was of particular interest to see if systematics with respect to geometry and well depths can be found. Initially, our analysis used six variable parameters,[3] but it became apparent that six-parameter fits to the data were more ambiguous and (again with the exception of C^{12}) not noticeably better than four-parameter fits. Even for the latter, some ambiguities remain. They have been investigated and are discussed below.

II. EXPERIMENTAL PROCEDURE

A. Targets

The targets used in this study were thin carbon-backed films of lithium, calcium, or titanium, and self-supporting carbon and aluminum foils.

The Al^{27} target thickness was measured by Rutherford scattering of 18-MeV O^{16} ions at $\theta_{lab} = 20$ and 30° and found to be 175 ± 10 $\mu g/cm^2$.

The carbon target was a thin, commercially prepared foil similar to those used as target backings. The thickness was measured by elastic scattering of 15-MeV protons, which was compared with the cross sections for $C^{12}(p,p)C^{12}$ measured by Daehnick and Sherr.[4] The calculated thickness was 27 ± 3 $\mu g/cm^2$, in good agreement with the nominal thickness of 30 $\mu g/cm^2$.

The lithium, calcium, and titanium targets were prepared by evaporation of the metals onto carbon backings. The titanium target, 97% enriched in Ti^{48}, was evaporated with an electron gun in a standard target preparation chamber and had a thickness of ≈ 40 $\mu g/cm^2$, as determined by Coulomb scattering. Calcium targets were prepared in the same way using natural calcium (97% Ca^{40}) or calcium fluoride.

The titanium targets withstood the O^{16} beam, but deteriorated after prolonged exposure to air. Calcium metal targets deteriorated quite badly when exposed to air while the calcium fluoride targets survived well.

The Li^7 target was made with natural lithium (93% Li^7) while the Li^6 target was prepared from 96% enriched Li^6. Lithium targets deteriorate after a few minutes exposure to air because of reactions with water vapor, hence our standard target preparation chamber could not be used. A small *in situ* evaporating system was built to fit on top of our 18-in. scattering chamber[5] (Fig. 1). Carbon foils were mounted on target frames which were raised from the scattering chamber into the evaporating system. Hence, targets could be lowered after evaporation into the beam line without further handling and without being exposed to air. Lithium and calcium target materials were evaporated from Monel metal or aluminum-oxide crucibles heated by a tungsten coil. The evaporating system was pumped by a liquid-nitrogen cold trap and by the vacuum of the scattering chamber, which maintained the pressure in the evaporator at $\sim 10^{-4}$ Torr during use. This very marginal vacuum resulted in considerable oxygen contamination,

but target damage due to water vapor was eliminated. For improved vacuum further pumping through the liquid-nitrogen trap is needed.

Since it was not possible to estimate the amount of target material deposited on the carbon backings accurately, the thickness of the targets was measured by the elastic scattering. For Li we used scattering of 9.80-MeV protons. The target thickness was computed by comparison of elastic proton scattering with the Li(p,p)Li cross sections given by Hintz.[6]

B. Detectors

Scattered O^{16} ions were detected with thin, fully or partially depleted silicon counters. Arrays of two to four counters were mounted on a cooled (−30°C) turntable at 10° intervals behind apertures ranging from ~0.1 to ~5 msr. Cooling allowed the use of higher than normal bias and improved charge collection. In order to limit kinematic broadening the detector apertures were limited to $\Delta\theta < 1°$. The detector thickness ranged from 60 to 300 μ for the fully depleted detectors. The partially depleted detectors had a thickness of 50 μ.

A thin Si detector was placed at $\theta = -15°$ inside the scattering chamber for monitoring purposes. At this angle contamination peaks were generally well resolved from the target peak. (Compare Fig. 2.) The comparison of elastic scattering into the monitor with the charge collected in the Faraday cup served to ascertain the stability of the target and the beam spot. The monitor to charge ratio was constant to within 10% for all accepted runs for a given target and energy.

The signals from all counters were amplified and routed into 512-channel groups of two Nuclear Data 4096-channel analyzers. Dead-time corrections were made by feeding the output of the charge integrator prescaler into the external clock input of the analyzers.

C. Effective Charge Corrections

The effective (average) charge carried by heavy ions emerging from a target depends almost entirely on the ion velocity once it has traversed a few $\mu g/cm^2$ of material.[7] It must be known accurately in order to properly normalize data which cannot be normalized to Rutherford scattering at small scattering angles. The effective charge of O^{16} ions of various energies has been measured for a number of materials[8] and a semiempirical relation between ion velocity and effective charge

TOP VIEW OF ON-LINE TARGET EVAPORATING SYSTEM

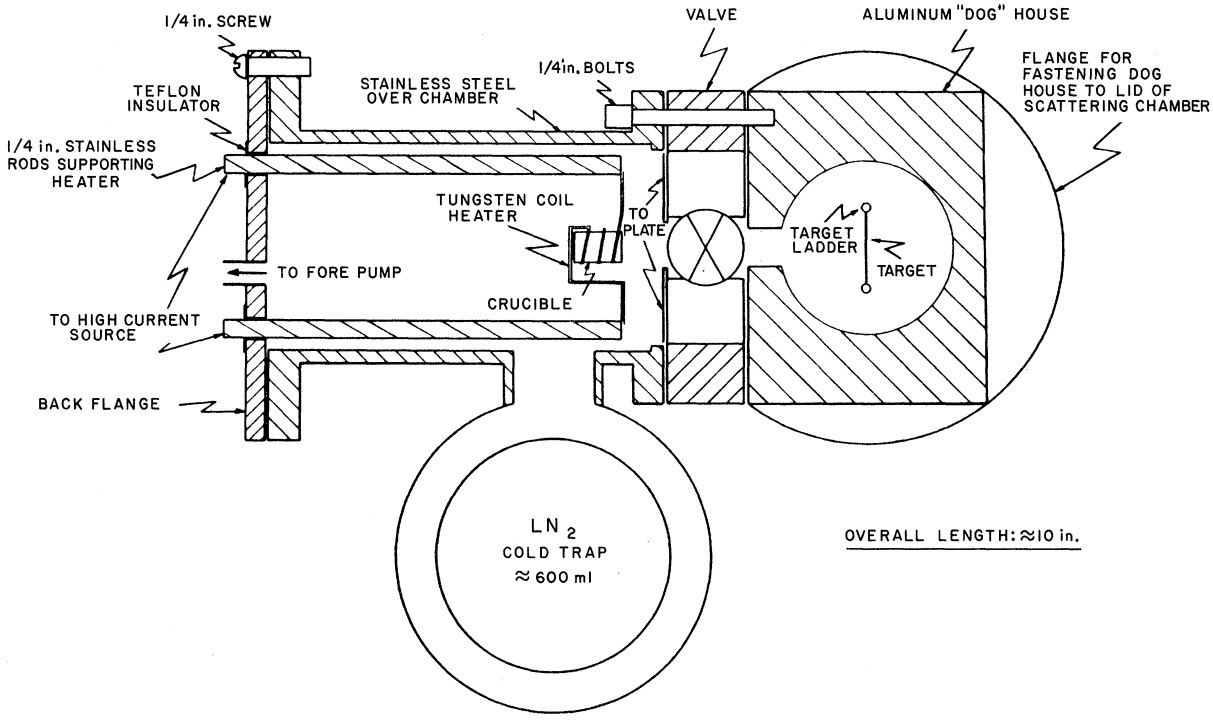

FIG. 1. The on-line evaporating system designed to fit onto the 18-in. scattering chamber. Upon completion of an evaporation targets are moved to the beam position ≈10 in. below.

has been given by Northcliffe.[9] The relation is $Z_{\text{eff}} = \gamma Z$, where Z is the atomic number of the ion, and $\gamma^2 = 1.85 - e^{-2\beta - \beta_k}$. $\beta = v/c$ is the velocity of the ion in the target and β_k is the "velocity" of an electron in the k Bohr orbit about the ion. The error of the effective charge correction from all sources was estimated to be ±5%.

III. EXPERIMENTAL RESULTS

Angular distributions presented start with the lowest angle at which it was possible to separate the impurity peaks from the elastic peak of interest, or for the self-supporting targets, the angle at which the beam began to graze the detector setup. The upper limits on θ were imposed by the presence of a low-energy very intense continuum (mostly α particles) which tended to bury the elastic peak at high angles. Some sample spectra are shown in Figs. 2 and 3.

A. $Li^{6,7}(O^{16}, O^{16})Li^{6,7}$

The Li^6 and Li^7 angular distributions are shown in Fig. 4. The error bars reflect all known random errors, composed of statistical, monitor, and background correction errors, the latter being most significant at larger angles. The error in the absolute scale normalization is not shown. It is primarily due to the uncertainty in target thickness, and is estimated at about 15%.

B. $C^{12}(O^{16}, O^{16})C^{12}$

The C^{12} data are displayed in Fig. 5. The errors shown are due to statistical and random monitoring errors. The scale error in the absolute cross section is ≈10%, and arises from the uncertainty in calculating the target thickness from the C^{12}-$(p,p)C^{12}$ cross sections and from the uncertainty in the O^{16} effective charge.

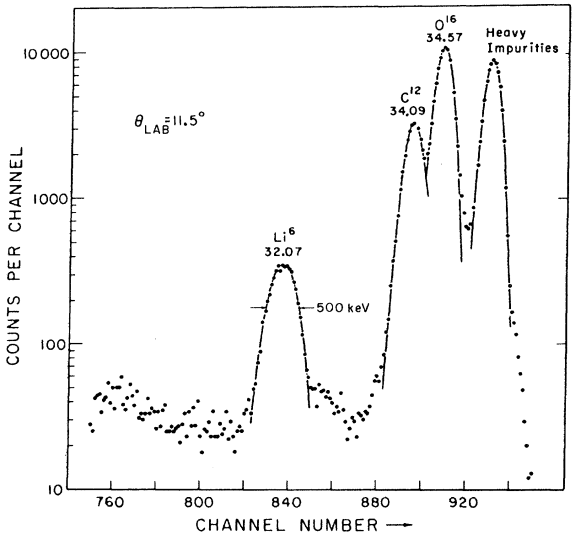

FIG. 2. A spectrum of elastically scattered O^{16} ions for a Li^6 target and $E_{O^{16}} = 36$ MeV. Heavy contaminants are due to impurities in the carbon backing and to Freon traces from the chamber cooling system.

C. $Al^{27}(O^{16}, O^{16})Al^{27}$

The Al^{27} angular distributions for 42 and 47 MeV are shown in Fig. 6. The angular distributions were normalized by Rutherford scattering at $E_{O^{16}} = 18$ MeV. The error bars are due to statistics and random monitoring errors. The absolute scale is believed to be correct to ≲10%. $Al^{27}(O^{16}, O^{16})$ excitation functions were taken for $36 \leq E \leq 42$ MeV at $\theta_{c.m.} = 55$ and 70°. No energy fine structure was observed.

D. $Ca^{40}(O^{16}, O^{16})Ca^{40}$ and $Ti^{48}(O^{16}, O^{16})Ti^{48}$

The Ca^{40} and Ti^{48} angular distributions are shown in Figs. 7 and 8, respectively. Inelastic scattering to the 2^+ first excited state of Ti^{48} was analyzed at $E_{O^{16}} = 42$ MeV and is shown in Fig. 9. The elastic scattering was normalized to Rutherford scattering at small angles and the absolute scale errors are ≲10%. Random errors are shown in the figures and are due to statistical errors and random monitoring errors.

Excitation functions were measured for Ca^{40} at $\theta_{c.m.} = 55$, 68, and 80° in 200-keV steps between 36 and 42 MeV. The measured values of $\sigma(E)$ were found to change smoothly with E within the relative (6%) experimental errors. This agrees well with the essentially structureless fall-off reported previously for this energy region[10] and indicates

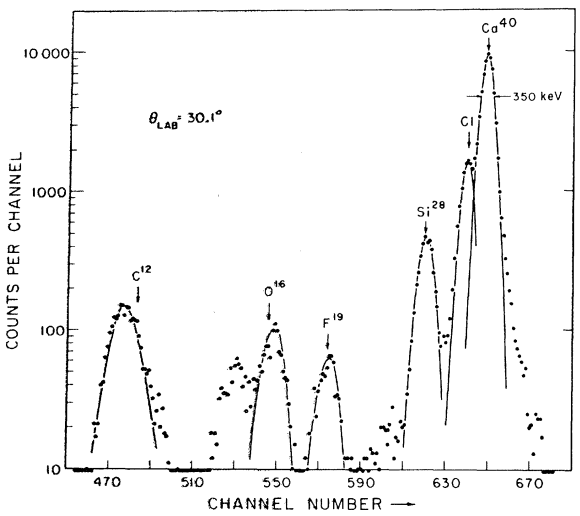

FIG. 3. A typical spectrum of $Ca^{40}(O^{16}, O^{16})Ca^{40}$ at $E_{O^{16}} = 40$ MeV.

that the coarse (1 MeV) steps used in Ref. 10 were not responsible for the apparent absence of fine structure. The excitation functions for Ca^{40} and Al^{27} are displayed in Fig. 10.

IV. OPTICAL-MODEL CALCULATIONS

Various attempts have been made to reproduce heavy-ion elastic scattering cross sections with the conventional and/or a modified[1,2,10-12] optical model. In this study conventional optical-model calculations were performed with code HUNTER[13] in order to find optimum parameters and to examine ambiguities in the parameters.

A. Procedure

Standard four-parameter Woods-Saxon and six-parameter derivative Woods-Saxon potentials were used:

$$U = -(V + iW)f(r) + V_{\mathrm{Coul}}(r) \ , \tag{1}$$

or

$$U = -Vf(r) + 4a' iW_D \frac{df'(r)}{dr} + V_{\mathrm{Coul}}(r) \ , \tag{2}$$

where

$$f(r) = \left[1 + \exp\frac{r - R_0 A^{1/3}}{a}\right]^{-1} \ ; \tag{3}$$

and

$$\begin{aligned} V_{\mathrm{Coul}} &= \frac{ZZ'e^2}{r} && r \geq R_c \\ &= \frac{ZZ'e^2}{2R_c}\left[3 - \left(\frac{r}{R_c}\right)^2\right] && r < R_c \ , \end{aligned} \tag{4}$$

where k is the wave number of the O^{16} ion in the center-of-mass system and r the distance from the scattering center. In view of the known[14] $V \cdot f(R)$ ambiguity the values of $R = R_0 A^{1/3}$ for the parameters finally used (Table I) were chosen to be the sum of the "classical" radius of O^{16} plus target radius, $R_0 A^{1/3} \equiv 1.3(A^{1/3} + 16^{1/3})$ fm. However, in the cases of Li^6, Li^7, and C^{12} it was found to be necessary to allow R_0 to vary somewhat in order to obtain the best fit to the data. R_c was kept fixed at $1.3A^{1/3}$, as the cross sections were not sensitive to it.

Code HUNTER has provision for matching the O^{16} wave function near the nucleus to a Coulomb wave function at a maximum "radius" of $kr \approx 65$ and this

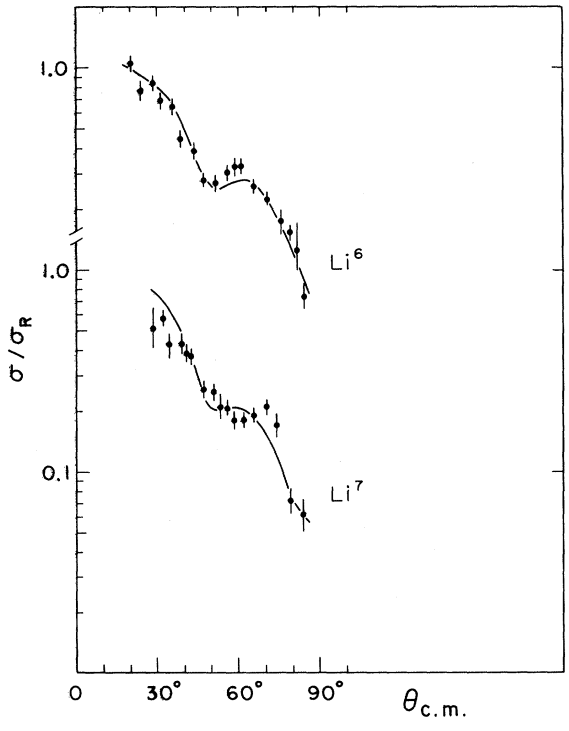

FIG. 4. The elastic cross section of $Li^{6,7}(O^{16}, O^{16})Li^{6,7}$ at $E_{O^{16}} = 36$ MeV. The error bars reflect random and statistical errors. Solid lines are optical-model fits to the data. The parameters are listed in the table.

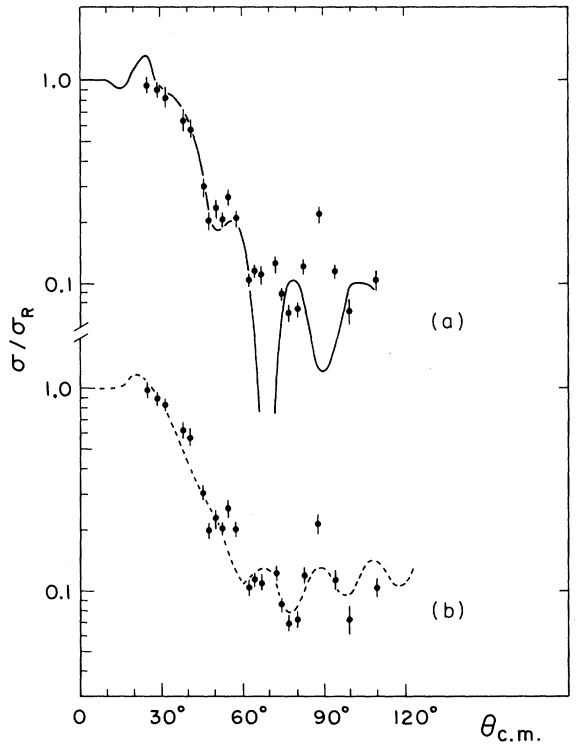

FIG. 5. The elastic cross section of $C^{12}(O^{16}, O^{16})C^{12}$ at $E_{O^{16}} = 36$ MeV. The solid line (a) is an optical-model fit with a four-parameter potential. The dashed line (b) shows the best fit to the $C^{12}(O^{16}, O^{16})C^{12}$ elastic cross section with a six-parameter potential. (Compare with the table.)

value was used for all calculations. Typical values of $kR_0A^{1/3}$ were between 20 and 30 and typical values of ka were 1.5 to 2. Thus the nuclear potential at the matching radius had fallen to $\sim 10^{-8}$ of its value at the nuclear surface. The use of a smaller matching "radius" $kr = 50$, was found to have negligible effect on the calculated cross sections. Since $kr \approx l$, the fixed matching radius corresponded to the 65th partial wave, which is well above the 40 partial waves carried in these calculations.

The rapid oscillation of the wave function near the origin requires a small integration step size to ensure accuracy. A step size of $\Delta(kr) = 0.1$ was used. An increase of $\Delta(kr)$ to 0.2 had a negligibly small effect on the calculations.

B. Results

It was found that the experimental data could be fit fairly well with the four-parameter potential except for C^{12}, which was fit poorly at larger angles [Fig. 5(a)]. The C^{12} fit with a six-parameter potential [Fig. 5(b)] does not look much superior, although the $\langle\chi^2\rangle$ value decreased markedly. The optical-model parameters and $\langle\chi^2\rangle$ values, with

$$\langle\chi^2\rangle \equiv \frac{1}{N}\sum_i \left(\frac{\sigma^i_{\text{th}} - \sigma^i_{\text{exp}}}{\Delta\sigma^i_{\text{exp}}}\right)^2 ,$$

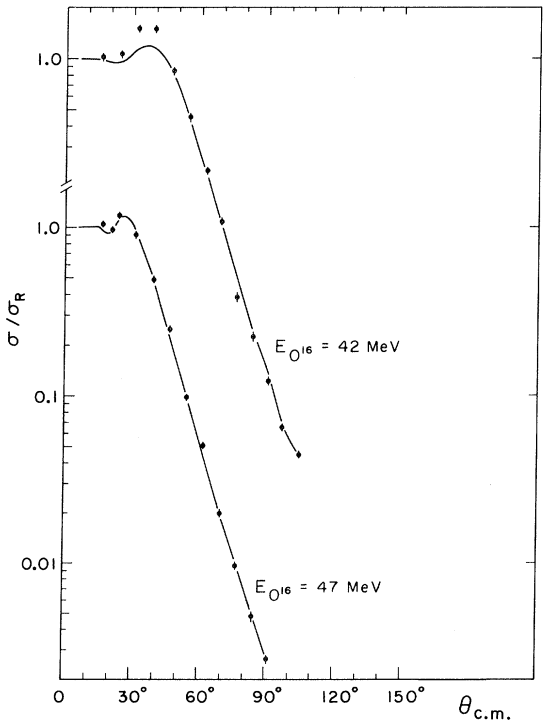

FIG. 6. The elastic cross sections of $Al^{27}(O^{16}, O^{16})Al^{27}$ at $E_{O^{16}} = 42$ and 47 MeV. Solid lines are four-parameter optical-model fits.

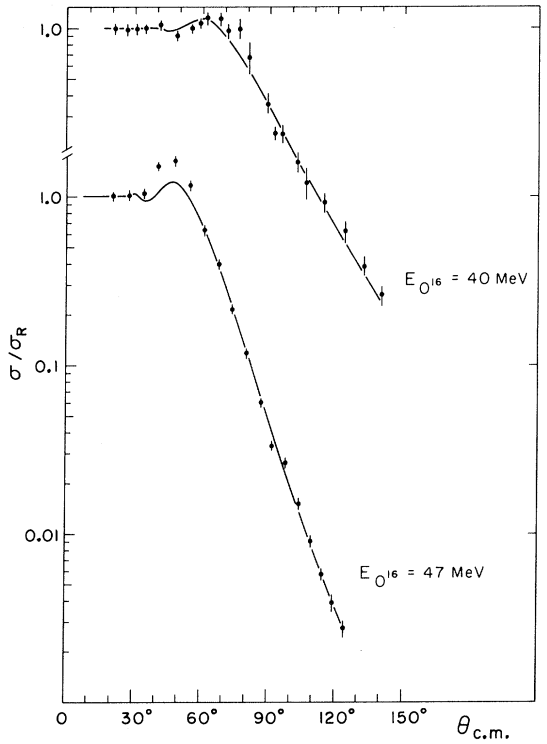

FIG. 7. The elastic cross sections of $Ca^{40}(O^{16}, O^{16})Ca^{40}$ at $E_{O^{16}} = 40$ and 47 MeV. Solid lines are four-parameter optical-model fits.

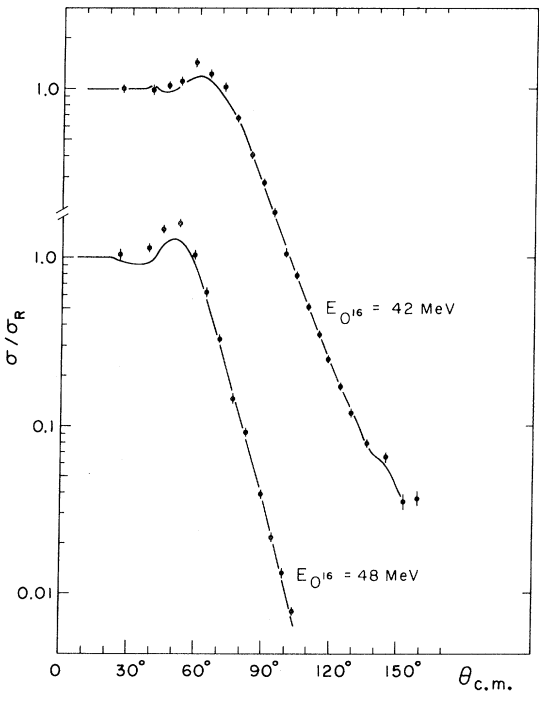

FIG. 8. The elastic cross sections of $Ti^{48}(O^{16}, O^{16})Ti^{48}$ at $E_{O^{16}} = 42$ and 48 MeV. Solid lines are four-parameter optical-model fits.

TABLE I. Best-fit optical parameters for O^{16} scattering. The choice of R_0 is explained in the text. σ_T is the total predicted reaction cross section in mb.

Target	$E_{lab}(O^{16})$ (MeV)	V (MeV)	W (MeV)	$4W_D$ (MeV)	R_0 (fm)	R (fm)	R_0' (fm)	a (fm)	a' (fm)	$\langle\chi^2\rangle$	σ_T (mb)
Li^6	36	10.1	3.32	...	2.296	4.14	...	0.649	...	1.2	463
Li^7	36	10.5	3.38	...	1.965	3.76	...	0.658	...	3.1	396
C^{12}	36	92.3	...	71.4	1.92	4.39	2.78	0.850	0.263	3.8	1044
C^{12}	36	51.3	2.45	...	2.73	6.24	...	0.533	...	22.0	893
Al^{27}	42	60.0	8.02	...	2.392	7.17	...	0.438	...	5.2	1005
Al^{27}	47	44.9	24.74	...	2.392	7.17	...	0.522	...	1.7	1303
Ca^{40}	40	91.7	43.7	...	2.258	7.72	...	0.406	...	0.88	572
Ca^{40}	47	62.9	4.46	...	2.258	7.72	...	0.399	...	1.9	797
Ti^{48}	42	60.3	3.05	...	2.201	8.0	...	0.418	...	0.47	583
Ti^{48}	48	60.2	3.38	...	2.201	8.0	...	0.403	...	3.1	838

are given in the table. Also shown are the predicted total reaction cross sections σ_T.

In performing the optical-model fits for the three heavier targets (Al, Ca, Ti) it was found that if well depth and geometry were related by

$$Ve^{R/a} = C_1 = \text{const.} \ , \tag{5a}$$

the fourth parameter, W, could be adjusted so that $\langle\chi^2\rangle$ remained essentially constant over the range 20 MeV $\lesssim V \lesssim$ 220 MeV. Hence, one parameter is arbitrary, and the values R_0 in the table could be derived from the classical target and projectile radii, with only V, W, and a as free fitting parameters. It was noted that for a = const., W and V were related in a particularly simple way by

$$W = A + BV \ , \tag{5b}$$

with A and B constants, which differ for each target and energy. This is shown for Al^{27} with $E_{O^{16}}$

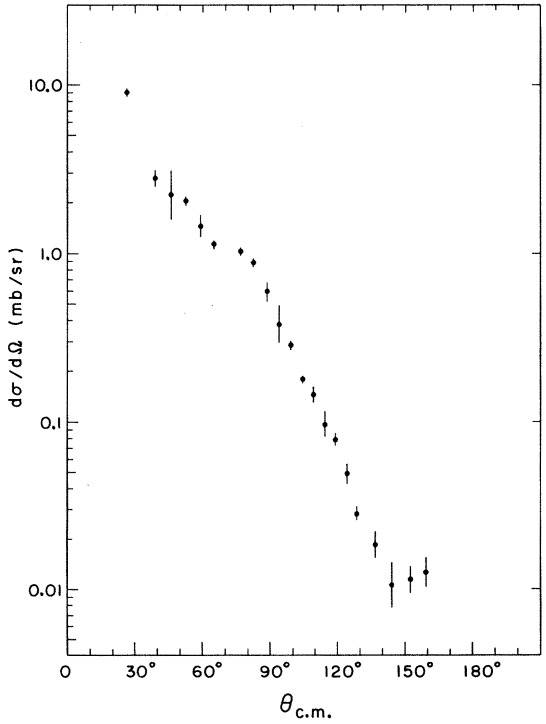

FIG. 9. The inelastic cross section of $Ti^{48}(O^{16}, O^{16})$-Ti^{48*} to the 2^+ level of Ti^{48} at 0.99 MeV. $E_{O^{16}} = 42$ MeV.

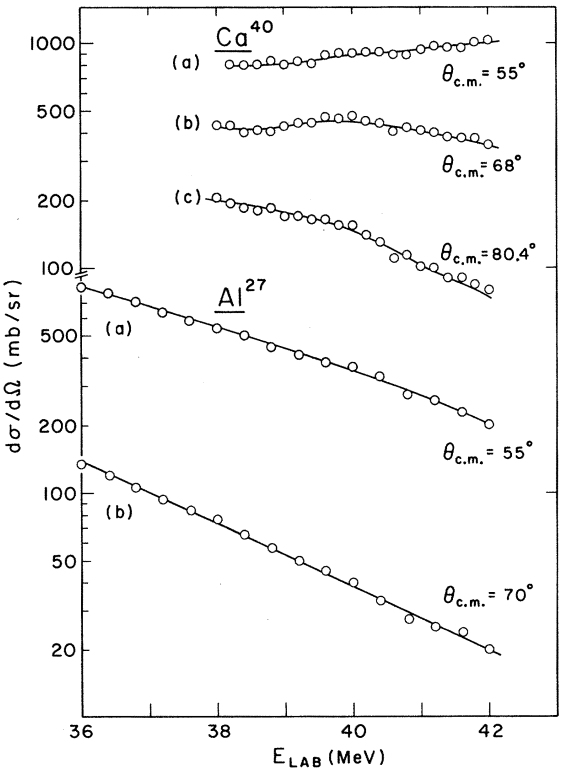

FIG. 10. Excitation functions for the elastic scattering of O^{16} by Al^{27} and Ca^{40} at various angles. The statistical errors do not exceed the size of the symbols; however, some small (<10%) but unknown additional errors due to target deterioration or beam spot instability may be present.

= 47 MeV in Fig. 11. The curves were generated by varying V and R_0 according to (5a) and allowing the code HUNTER to vary until $\langle\chi^2\rangle$ was minimized.

Figure 11 demonstrates that the $W(V, R_0, a)$ ambiguity appears to be truly continuous for Al^{27}-$(O^{16}, O^{16})Al^{27}$. A similar continuous ambiguity was initially suggested for elastic α scattering by Igo[14] who also proposed (5a). This condition essentially assures the invariance of the predicted reflection from the nuclear surface.[15] Igo argued that α scattering was insensitive to the nuclear interior. Although this view was later modified by Drisko, Satchler, and Bassel who showed[15] that for α scattering a true ambiguity existed only for discrete values of V, and who found no simple conditions for W, it is not surprising that Igo's arguments hold rather better for the more strongly absorbed O^{16} projectiles. Igo's postulate for W was[14] $We^{R_W/a_W} = C_2$. In our four-parameter model this leads to $W = C_3V$. Our empirical condition (5b) differs by an additive constant A, but agrees with the proposed linear relationship of V and W for elastic O^{16} scattering by Al^{27}, Ca^{40}, and Ti^{48}.

Comparison of data and fits for the latter targets show pronounced energy dependent peaks in the σ/σ_R plots (Figs. 6–8), which in at least three of the six angular distributions are only qualitatively reproduced by the optical-model fits. The frequent occurrence of this feature in nuclei for which competing reaction mechanisms are not likely to be strong and for which the measured angular distributions are extremely simple must be noted as a shortcoming of the conventional optical-model interpretation. It is extremely unlikely that the discrepancy is due to experimental errors.

V. DISCUSSION AND COMPARISON WITH OTHER WORK

For the isotopes investigated the data on C^{12}-$(O^{16}, O^{16})C^{12}$ and $Ca^{40}(O^{16}, O^{16})Ca^{40}$ (at 40 MeV) can be compared with previous work.[1,10] Assuming that the experimental errors in Ref. 10 are about 10% there is good agreement for Ca^{40} at 40 MeV. Reference 1 contains a rather extensive study of $O^{16} + C^{12}$ scattering at energies similar, but not identical to ours. Qualitative agreement is expected and seen. The data at slightly lower energies[1] offer the explanation needed for our failure to obtain satisfactory optical-model fits for C^{12}. Excitation functions for elastic scattering for $30 \leq E_{\text{lab}} \leq 35$ MeV show broad irregular fluctuations (factors of up to 3 from the average cross sections) at angles of 90° and larger,[1] which are indicative of sizeable nondirect scattering amplitudes. In addition there is evidence that for larger angles ($\theta \gtrsim 80°$) α-exchange amplitudes interfere with potential scattering.[1] Given these facts it would seem wrong to attach any particular significance to the C^{12} parameters extracted. It is interesting to note, however, that the four-parameter fit [Fig. 5(a)] gives a better account of forward-angle data, which should be dominated by potential scattering, than the six-parameter fit, which reproduces, qualitatively, the larger-angle structure. It is also worth noting that although our 36-MeV data are intermediate between the 35-

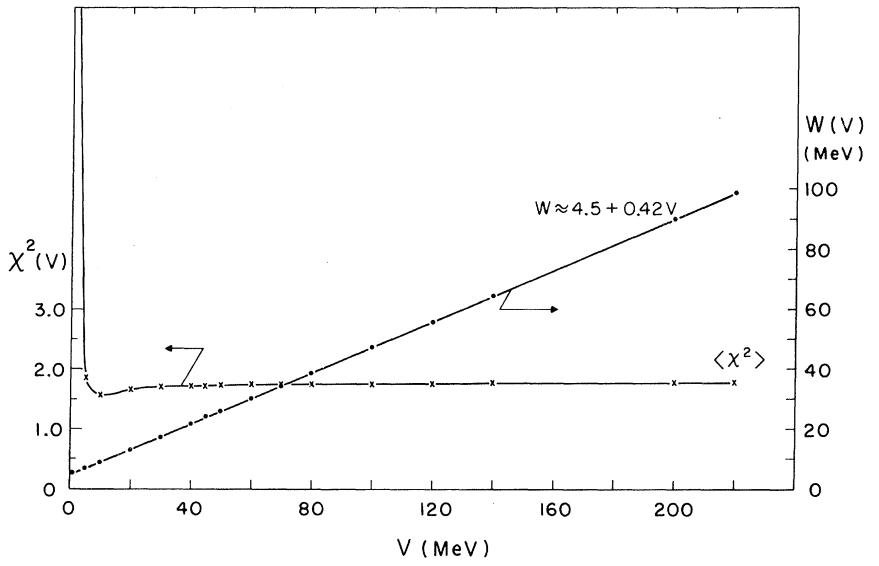

FIG. 11. Example of a continuous parameter ambiguity for optical-model fits. χ^2 and W plotted as functions of V for the elastic scattering of O^{16} from Al^{27} at $E_{O^{16}} = 47$ MeV. The four-parameter Woods-Saxon potential was used and V and R_0 were varied according to Eq. (5a) with $a = 0.552 = \text{const}$. The individual calculational points are shown.

and 42-MeV data of Ref. 1, they are more similar to the latter in gross structure. In particular, between 30 and 65° the 35-MeV cross-section ratio σ/σ_R drops from 1.2 to 0.4, while for 36 MeV we see a drop from 0.9 to 0.11. For the 42-MeV data[1] the "65° minimum" has moved to ~50° and the drop of σ/σ_R is from 1.0 to 0.08. The rapid variation of the $C^{12}+O^{16}$ scattering from 35 to 36 MeV (lab) is one more indication that a quantitative theory for the $O^{16}+C^{12}$ interaction may be a long way off.

For the isotopes Li^6, Li^7, Al^{27}, Ca^{40}, and Ti^{50} the analysis in terms of potential scattering seems much more successful and appropriate. To begin with, exchange scattering amplitudes would involve the transfer of seven or more nucleons and should be negligibly small. Also, the experimental cross sections seem to change smoothly with energy, hence compound effects may be small. Given the simple structure of $\sigma(\theta)$, it is not surprising that the $\langle\chi^2\rangle$ values for the four-parameter optical-model fits are small, and that the angular distributions are quite well reproduced. Considering that the optical well geometry was held nearly constant with only a small variation in a, $0.40 \leq a \leq 0.66$, the variation in V seems reasonable. The behavior of W is less satisfactory from the optical-model point of view in that the parameter fluctuates and often seems too small in view of the strong absorption expected on physical grounds. It is possible – on account of the continuous ambiguities outlined above – to decrease R_0 and still produce good fits with larger values for V and W, but an arbitrary variation of R_0 seems equally unsatisfactory.

The erratic behavior of W with E for Al^{27} and Ca^{40} and the failure to predict or fit the considerable (20 to 70%) peak in σ/σ_R before its steep fall-off indicates the need for some extension or change of the optical model for heavy-ion scattering, conceivably along the lines suggested in Refs. 2 and 10. The introduction of the l cutoff factor $f(l) = \{1+\exp(l-l_0)/(\Delta l)\}^{-1}$ for the imaginary potential has been tried for $Ca^{40}(O^{16}, O^{16})Ca^{40}$ at 40 MeV by Eck, LaSalle, and Robson,[10] who state that this factor improved the fits obtainable for Ca^{40}. It must be pointed out, however, that the fits published in Ref. 10 seem quite inferior to the one given here [Fig. 7(a)]. (A more precise statement cannot be made as Ref. 10 gives neither experimental errors nor χ^2 values for the fits.) This surprising outcome may have been caused by the use of a more efficient search routine (HUNTER[13]) in this work or by a less than optimum choice[12] of the cutoff parameters l_0 and Δl in Ref. 10.

A comparison of the optical-model parameters extracted in this and previous work can be made only in general terms: (1) We find as other studies[1,10,12] have before that a fit with shallow potentials ($10 < V < 20$ MeV) seems always possible and sometimes (Li^6, Li^7) preferred[16] if realistic geometries are used. (2) For all but the lightest isotopes we find continuous ambiguities that permit values for V up to 200 MeV or higher, where larger values of V require larger values for W. (3) The optical-model parameters extracted in this work and Ref. 10 for Ca^{40} do not belong to the same type potential; they are not related by Eq.(5a).

We conclude that there is not yet an optical-model prescription for heavy ions which permits realistic interpolation for E or A, and much extra work need still be done. However, frequently optical-model potentials with three or four free parameters can be found that are of a quality adequate to correctly yield the important phase shifts for heavy-ion scattering for a given target and O^{16} energy.

---

†Work supported by the National Science Foundation.

[1]U. C. Voos, W. Von Oertzen, and R. Bock, Nucl. Phys. A135, 207 (1969), and references therein.

[2]R. A. Chatwin, J. S. Eck, D. Robson, and A. Richter, Phys. Rev. C 1, 795 (1970).

[3]J. Orloff and W. W. Daehnick, Bull. Am. Phys. Soc. 13, 650 (1968).

[4]W. W. Daehnick and R. Sherr, Phys. Rev. 133, B934 (1964).

[5]R. H. Fulmer and W. W. Daehnick, Phys. Rev. 139, B579 (1965).

[6]N. M. Hintz, Phys. Rev. 106, 1201 (1957).

[7]E. L. Hubbard and E. J. Lauer, Phys. Rev. 98, 1814 (1955).

[8]H. H. Hechman, E. L. Hubbard, and W. G. Simon, Phys. Rev. 129, 1240 (1963); K. G. Stephens and D. Walker, Proc. Roy. Soc. (London) A229, 376 (1955); V. S. Nikolaev *et al.*, Zh. Eksperim. i Teor. Fiz. 33, 1325 (1957) [transl.: Soviet Phys. – JETP 6, 1019 (1958)]; R. A. Brown and G. D. Symons, Nucl. Instr. Methods 58, 274 (1968).

[9]L. C. Northcliffe, Phys. Rev. 120, 1744 (1960).

[10]J. S. Eck, R. A. LaSalle, and D. Robson, Phys. Rev. 186, 1132 (1969).

[11]G. H. Rawitscher, J. S. McIntosh, and J. A. Polak, in *Proceedings of the Third International Conference on Reactions Between Complex Nuclei, Asilomar, California, 1963,* edited by A. Ghiorso, R. M. Diamond, and H. E. Conzett (University of California Press, Berkeley, California, 1963).

[12]R. W. Shaw, Jr., R. Vandenbosch, and M. K. Metha, Phys. Rev. Letters 25, 457 (1970).

[13]Written by R. M. Drisko, unpublished. We are grateful to Professor Drisko for permission to use his code HUNTER, and for valuable discussion about the optical model.

[14]G. Igo, Phys. Rev. 115, 1665 (1959); Phys. Rev. Letters 1, 2 (1958).
[15]R. M. Drisko, G. R. Satchler, and R. H. Bassel, Phys. Letters 5, 347 (1963). See also, N. Austern, Ann. Phys. (N.Y.) 15, 299 (1961).
[16]J. V. Maher, M. W. Sachs, R. H. Siemssen, A. Weidinger, and D. A. Bromley, Phys. Rev. 188, 1665 (1969).

PHYSICAL REVIEW C VOLUME 3, NUMBER 2 FEBRUARY 1971

Mass and Half-Life of ^{9}C†

J. M. Mosher, R. W. Kavanagh, and T. A. Tombrello
California Institute of Technology, Pasadena, California 91109

(Received 9 October 1970)

The mass of ^{9}C has been measured by counting delayed protons near the ^{7}Be(^{3}He, n)^{9}C threshold. The data are consistent with an s-wave threshold at $E_{^3\mathrm{He}} = 8980 \pm 5$ keV, giving a ^{9}C mass excess of $28\,907 \pm 4$ keV, and confirming the reported deviation of the $A = 9$, lowest $T = \frac{3}{2}$ quartet from the quadratic mass formula. The half-life of ^{9}C, measured with a multiscaler, is 126.5 ± 2 msec.

The ground states of ^{9}C and ^{9}Li together with the $T = \frac{3}{2}$ excited states at 14.392 MeV in ^{9}Be and at 14.655 MeV in ^{9}B have been the subjects of considerable investigation because they form one of the few presently accessible isospin quartets. This experiment was undertaken to attempt to verify and improve the measurement of the ^{9}C mass. The experimental method of deducing that quantity from the threshold energy of the ^{7}Be(^{3}He, n)^{9}C reaction had been used previously by Barnes *et al.*[1]

A ^{7}BeO target, prepared for an earlier experiment[2] by evaporating under vacuum a $\frac{1}{8}$-in.-diam spot of $^7BeF_2$ onto a 1.2-mm-thick platinum bar and then oxidizing the layer in air, provided a surface density of 7×10^{16} ^{7}Be atoms per cm^2. This number represents about half of the ^{7}Be present when the target was first prepared, the other half having decayed to ^{7}Li, which, along with the oxygen and other impurities, contributed to a measured target thickness of 10 keV for the 9-MeV ^{3}He^{++} beam supplied by the Office of Naval Research-California Institute of Technology tandem Van de Graaff accelerator near the reaction threshold.

The target was mounted in a chamber[2] equipped with a solenoid-operated arm capable of switching the target between a beam line and a counting position in an 873-msec cycle. For the first 290 msec of each cycle, the target spot was exposed to $\sim\frac{1}{2}$ μamp ^{3}He. If ^{9}C was formed, it would be expected to β^+ decay into the broad particle-unstable states of ^{9}B, which almost immediately break up into a proton plus ^{8}Be. Thus, in the second part of the cycle, after the beam had been deflected, the target was moved directly in front of a $\Delta E + E$ telescope consisting of an 11- and a 26-μm silicon detector, with a geometrical efficiency of ~15%. This arrangement of counters was necessary in order to be able to sort out the protons accompanying ^{9}C decays from the intense background of 478-keV γ rays emitted by the 50 mCi of ^{7}Be, as well as from the α particles and other activity induced by the ^{3}He bombardment. When a pulse from the ΔE counter consistent with a proton energy loss of 0.27–0.55 MeV arrived in coincidence with a pulse from the E counter large enough to be distinguished from the γ-ray background, the sum was recorded by a multichannel analyzer. The natural radioactivity of the target restricted both the choice of detector volume and the smallest ΔE (largest proton energy) that could be accepted. Two successive counting periods of 229 msec each were recorded separately to provide a check of the half-life.

Figure 1 shows the sum of the spectra obtained during the 16 threshold runs. The broad group of protons with 0.75–3.0-MeV energy loss in the counters is clearly separated from the constant γ-ray background at the low-energy end. Because some of the delayed protons had ranges greater than the total thickness of the two detectors and/or values of ΔE outside our 0.27–0.55-MeV window, the shape of the observed spectrum is essentially determined by the coincidence requirements rather than by the actual distribution of proton energies.

During a typical 40-min run, the target was exposed to an integrated beam current of 300 μC. The yield, taken as the sum of the counts accumulated in channels 27 through 100, varied with ^{3}He^{++} bombarding energy as shown in Fig. 2. If one assumes that $l = 0$ neutrons are emitted near thresh-